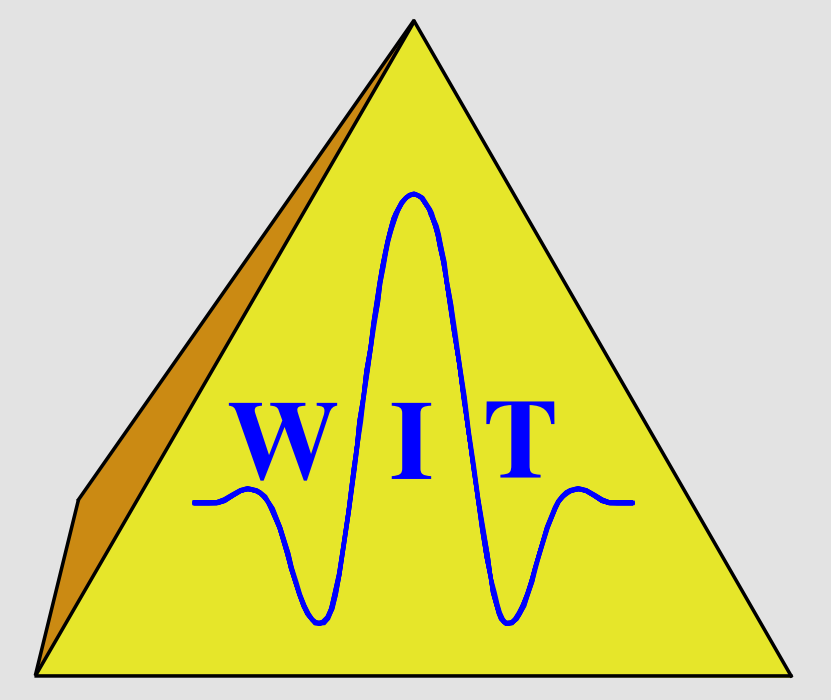


CRS-based minimum-aperture time migration – a real data example

Mareike Kienast, Miriam Spinner, and Jürgen Mann
Geophysical Institute, University of Karlsruhe, Germany



Summary

The achievable image quality and the reliability of amplitudes in Kirchhoff migration strongly depend on the selection of the migration aperture. Optimal amplitudes are obtained if the migration aperture is restricted to the constructively contributing part of the reflection event which is related to the size of the projected Fresnel zone. The Common-Reflection-Surface (CRS) stack provides kinematic wavefield attributes that allow to address this problem together with a straightforward time migration velocity model building. The approach is applied to a complex onshore data set and compared to conventional Kirchhoff migration. We observe an improved continuity of the reflection events as well as more stable amplitudes in regions with reliably detected CRS attributes. Moreover, the computational costs of the prestack migration are significantly reduced.

Introduction

The Common-Reflection-Surface (CRS) stack method provides a set of stacking parameters, so-called kinematic wavefield attributes, which can be utilised in subsequent processing steps. Jäger (2005) employed the CRS attributes in pre- and poststack Kirchhoff depth migration to estimate the size and location of the minimum migration aperture with the aim to reduce migration artifacts and to avoid operator aliasing. As depth migration is quite sensitive to velocity model errors and costly in terms of inversion, Spinner and Mann (2006) transferred the concept to the time domain. The focus of the time domain approach is to reduce migration artefacts and to provide an improved input for subsequent amplitude-versus-offset (AVO) analysis. In this paper, we present the first application of the approach to real data and a comparison to conventional results.

Basics of CRS stack

The CRS method is based on a second-order approximation of the kinematic reflection response of an arbitrarily curved reflector segment in depth. This approximation can be entirely expressed in terms of kinematic wavefield attributes defined at the acquisition surface rather than in the subsurface: in 2D, these are the emergence angle α of the central ray, and the radii R_{NIP} and R_N of wavefront curvature of two hypothetical waves, the so-called NIP and normal wave, respectively. The commonly used hyperbolic approximation can, e.g., be found in Schleicher et al. (1993). Similar to a conventional stacking velocity analysis, the optimum wavefield attributes for each location (x_0, t_0) are determined automatically by means of coherence analysis. The final results are entire sections of the wavefield attributes α , R_{NIP} , and R_N , as well as a coherence section.

Determination of stationary points

In Kirchhoff migration, the main contribution to the diffraction stack stems from the region where the reflection event is tangent to the migration operator, the vicinity of the so-called stationary point x_0 . As the CRS operator is already tangent to a reflection event in the data, this tangency condition can be directly evaluated by a comparison of the CRS operator slope and the migration operator slope. The searched-for slope β of the ZO reflection event is related to the emergence angle α of the ZO ray via the near-surface velocity v_0 : $\tan \beta = 2 \sin \alpha / v_0$. For time migration with straight rays as considered here, the migration operator as well as its derivatives are given by analytic expressions. In practice, the modulus of the difference between these two slopes is calculated and the location of the minimum is chosen as stationary point. The associated coherence values help to decide whether the stationary point is reliable by applying a user-given threshold.

The concept of the *Common-Reflection-Point (CRP) trajectory* allows to extrapolate the stationary point to finite offset. It is entirely defined in terms of the kinematic wavefield attributes (Höcht et al., 1999):

$$x_m(h) = x_0 + r_T \left(\sqrt{\frac{h^2}{r_T^2} + 1} - 1 \right), \quad (1a)$$

with

$$r_T = \frac{R_{NIP}}{2 \sin \alpha}. \quad (1b)$$

Equation (1a) represents the projection of the CRP trajectory onto the midpoint/offset plane. A similar expression for the traveltimes (not shown) is not required in this context.

The approximation provides a superior reference for the centre of the migration aperture compared to the conventional approach which ignores the deviation between Common-Midpoint (CMP) and CRP gathers.

Estimation of minimum aperture

The final information relevant for minimum migration apertures which can be gained from the attributes is the size of the projected ZO Fresnel zone W_F . According to Mann (2002) it can be expressed as

$$\frac{W_F}{2} = |x_m - x_0| = \frac{1}{\cos \alpha} \sqrt{\frac{v_0 T}{2 \left| \frac{1}{R_N} - \frac{1}{R_{NIP}} \right|}}. \quad (2)$$

In general, the Fresnel zone size is expected to widen with offset. Unfortunately, this effect is hard to quantify as the velocity model together with the dip and curvature of the reflector has to be considered. However, forward-calculated examples suggest that the widening effect is small for reflectors with moderate dip and curvature. For practical application, the ZO Fresnel zone size as determined from the CRS attributes is always extended by a certain percentage (usually 10 to 20% depending on the attribute quality) as it is crucial not to underestimate the Fresnel zone for true-amplitude processing. Thus, the small widening effect is already covered and may be neglected. For the data example below, the Fresnel zone was set constant for all offsets, an approximation which appears to be reasonably accurate to obtain reliable amplitudes in this case.

Real data example

To demonstrate the potential of true-amplitude CRS-based Kirchhoff time migration the approach was applied to a complex onshore data set. To gain the kinematic wavefield attributes the highly automated CRS stack method was applied to the real data set.

For the determination of the velocity model, attributes were automatically picked at 2870 data points with high coherence. Reliable picks could only be determined from CMP nos. 1 to 1225. Beyond this location the velocity model was constantly extrapolated in lateral direction. The interpolated velocity model is displayed in Figure 1. Some common-image gathers extracted from the conventional prestack migration result are shown in Figure 2. An offset-dependent moveout can be clearly observed for the right hand part of the model where, due to the lack of reliable picks, a constant extrapolation has been used.

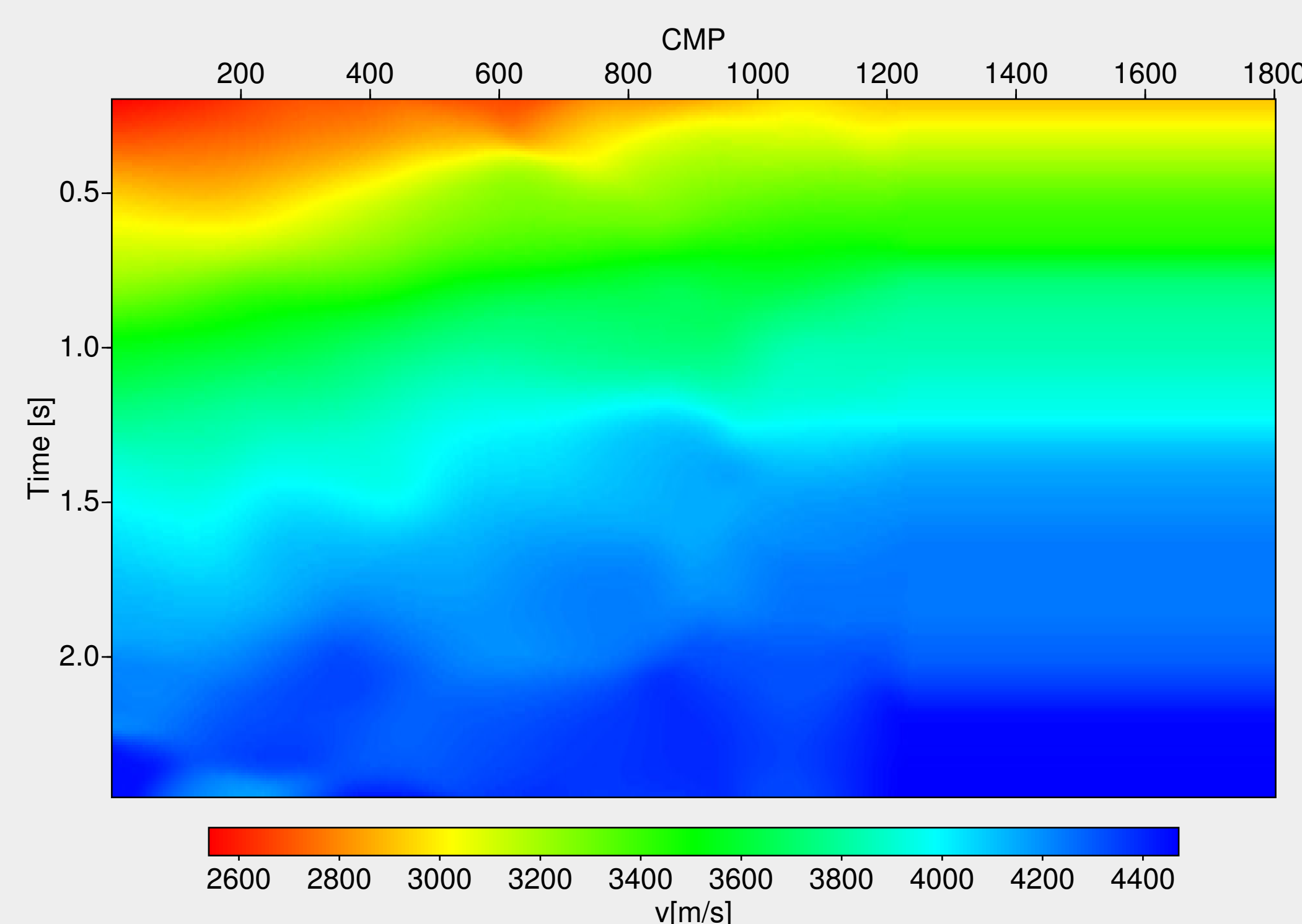


Figure 1: Smoothed time migration velocity model determined from the CRS wavefield attributes.

With the attribute-based time migration velocity model, true-amplitude Kirchhoff poststack time migration was performed twice: on the one hand in a conventional way with a user-defined aperture, on the other hand with the limited aperture given by the projected Fresnel zone. The poststack time migration was processed using the CRS stack section (not shown). The migration target zone consists of a grid with 25 m spatial and 4 ms temporal intervals. The high temporal resolution was chosen to allow a clear separation of closely adjacent reflection events.

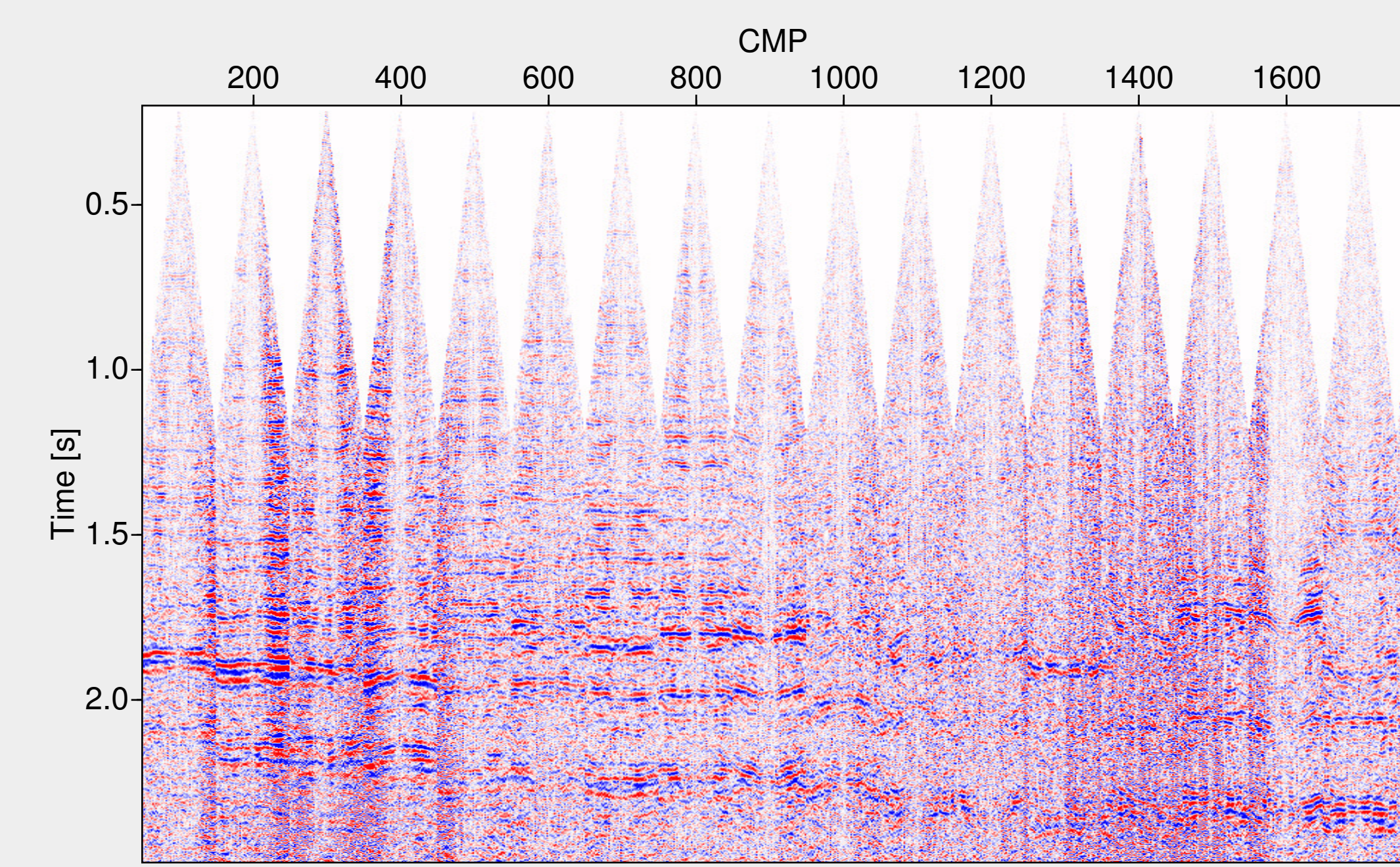


Figure 2: Several common-image gathers extracted from the conventional time migration prestack data. The maximum offset is 3 km.

For the data at hand, the conventional user-given aperture had to be chosen such that the steeply dipping reflector elements located between CMP nos. 500 and 750 and between 1000 and 1100 could be properly imaged. For both approaches a taper was considered in order to suppress artifacts due to border effects.

Projected Fresnel zone

For all locations where a stationary point has been detected, Figure 3 shows the projected Fresnel zone. As expected, its size increases with increasing traveltimes and increasing curvature of the reflection events.

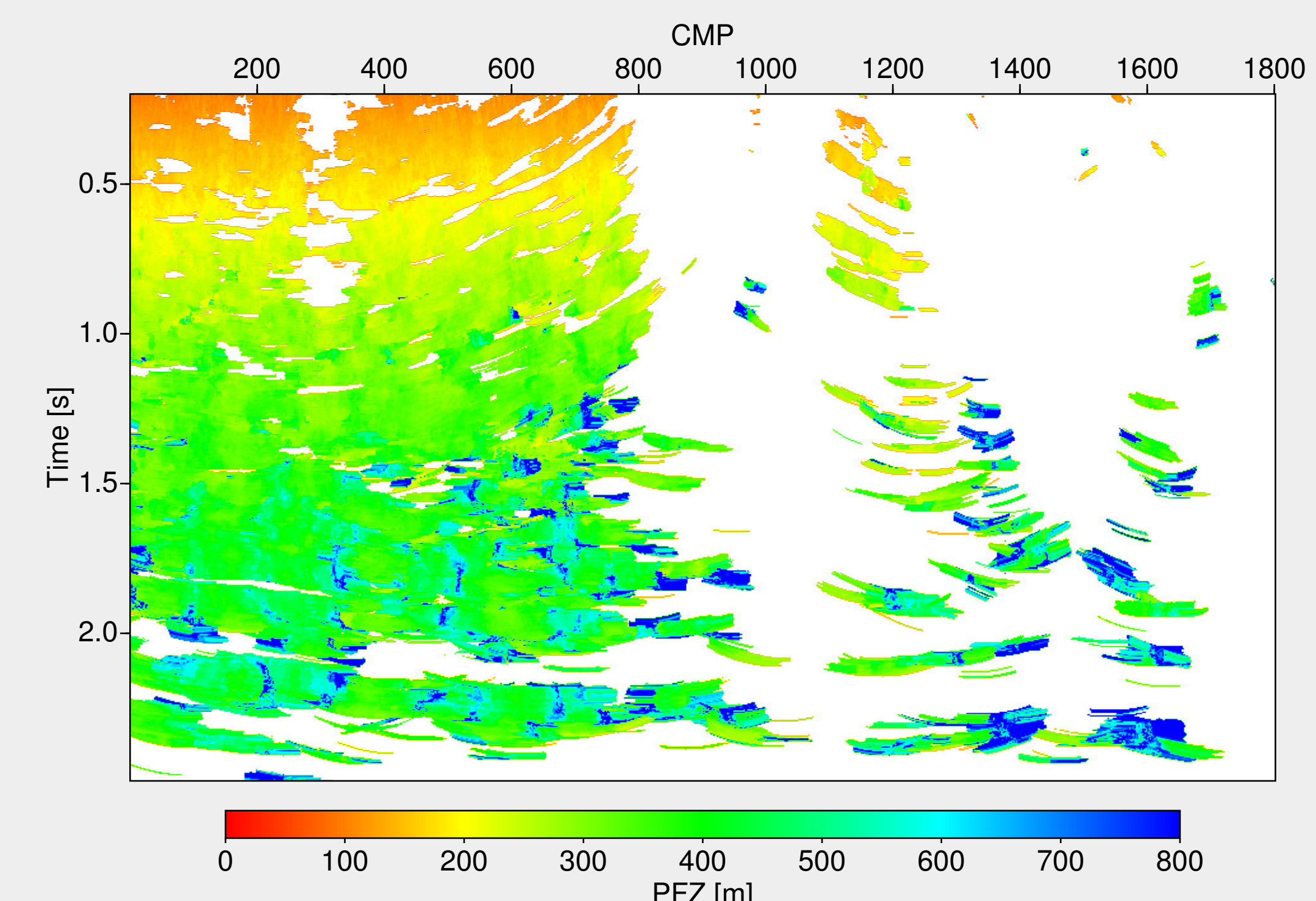


Figure 3: Size of the projected first ZO Fresnel zone estimated from the CRS attributes. Only locations with identified stationary points have been considered.

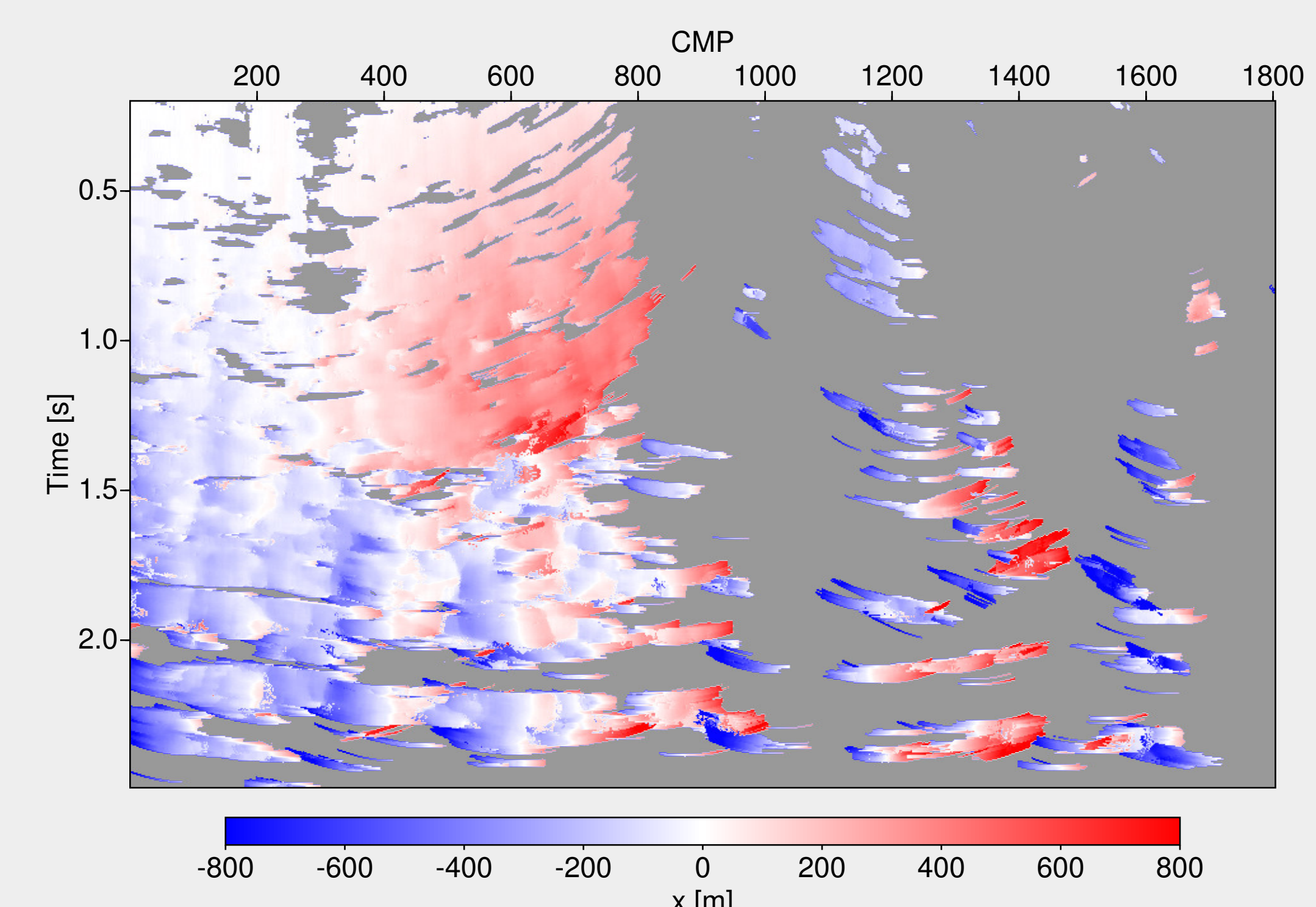
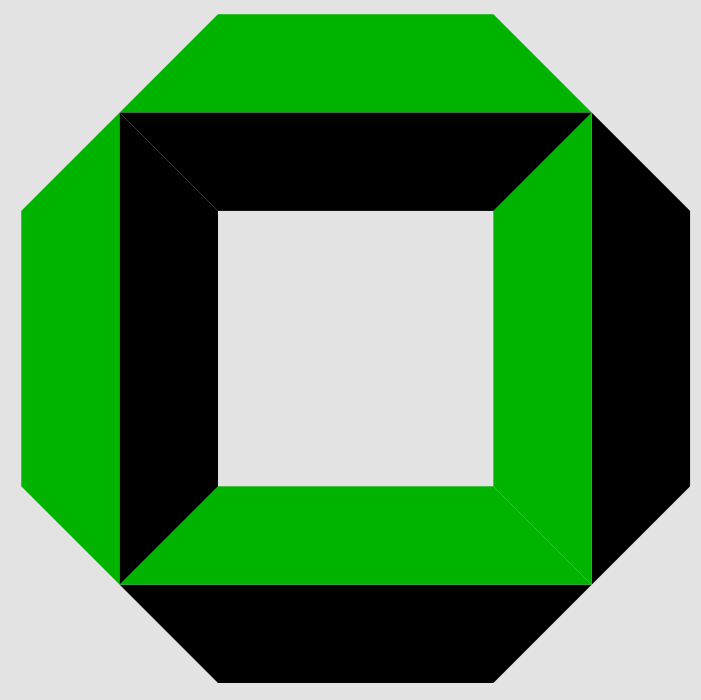


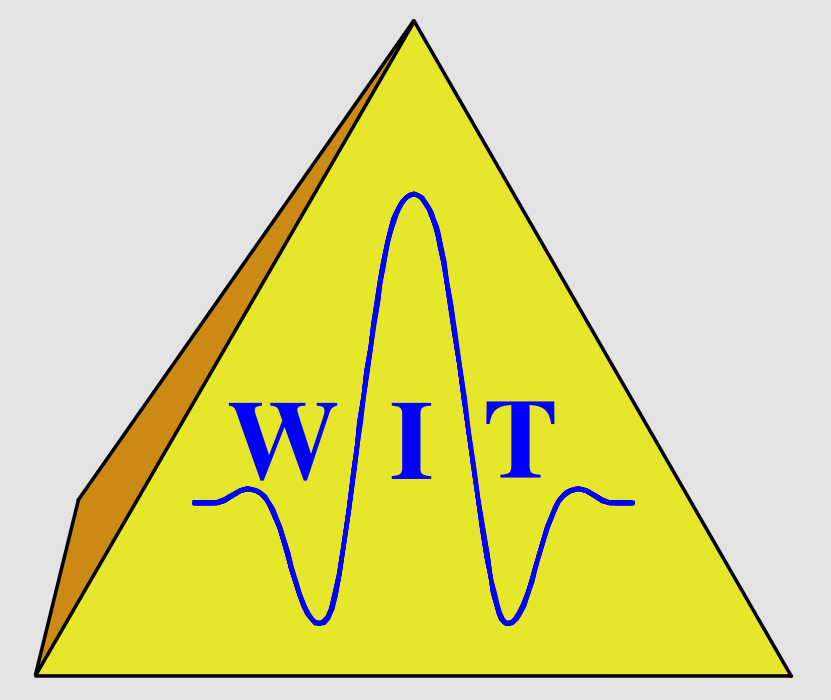
Figure 4: Horizontal distance between operator apex and stationary point estimated from the CRS attributes. Only locations with identified stationary points have been considered.

We observe conspicuously large projected Fresnel zones at various locations. To analyse this effect, we consider the Fresnel zone and the CRS attributes in the unmigrated domain. According to the relation between the Fresnel zone size and the CRS attributes, this indicates (fragments of) diffraction events with $R_N \approx R_{NIP}$. As at such locations there are no evident anomalies in the NIP wave radius which might indicate failures of the search algorithm, this interpretation appears consistent.



CRS-based minimum-aperture time migration – a real data example

Mareike Kienast, Miriam Spinner, and Jürgen Mann
Geophysical Institute, University of Karlsruhe, Germany



In Figure 4 the horizontal distance between operator apex and stationary point is depicted. It is clearly visible that for flat events the distance tends to zero while on steep events the values of the distance between operator apex and stationary point reach up to 800 m. This demonstrates why a large conventional user-defined aperture is required to capture such events.

For these data, conflicting dip handling has not been applied due to the poor signal-to-noise ratio. As a consequence, only one event can be characterised at each ZO location, namely the event associated with the highest coherence. As the steep flanks of (weak) diffraction events interfere with neighbouring reflection events, they often appear as fragments, only. Nevertheless, the local attributes clearly reveal their nature.

Poststack migration results

Figure 6 shows the results of the limited-aperture poststack migration. Where no stationary points have been detected, the user-defined aperture was utilised at such locations to obtain a fully covered image without gaps. For comparison, Figure 5 displays the result of the conventional poststack time migration. In the upper part of the two migrated images only minor differences can be seen, even for the events with significant dip. The good performance of the conventional approach in this area can be explained as follows: for the events with small dips, a comparatively small user-given aperture can be used without loss of events. The steeper events show a slightly concave structure that leads to a slight decrease in the Fresnel zone size. Therefore, the projected Fresnel zone is still well covered by the user-given aperture although it is displaced with respect to the operator apex.

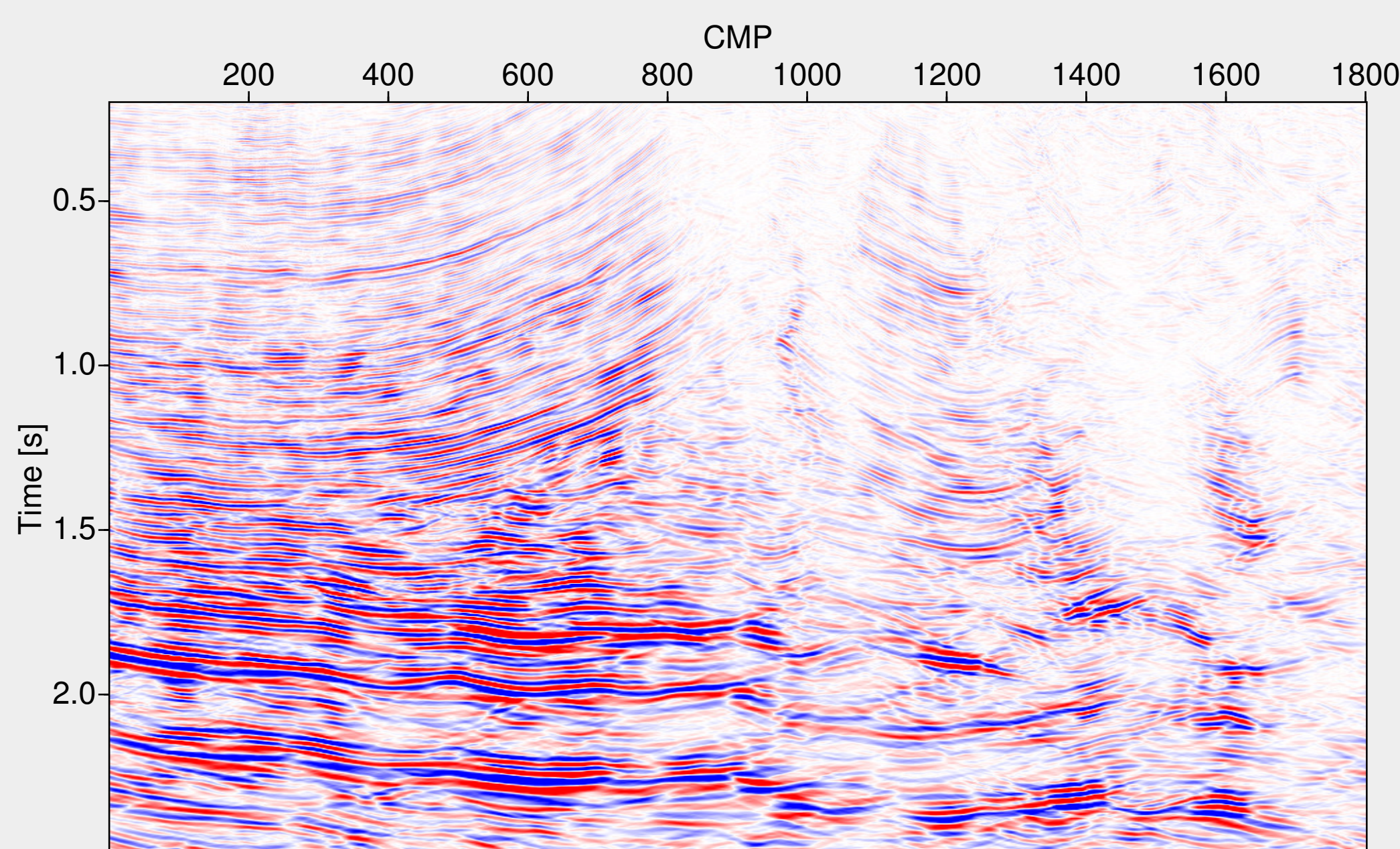


Figure 5: The result of the Kirchhoff poststack time migration with conventional user-defined aperture.

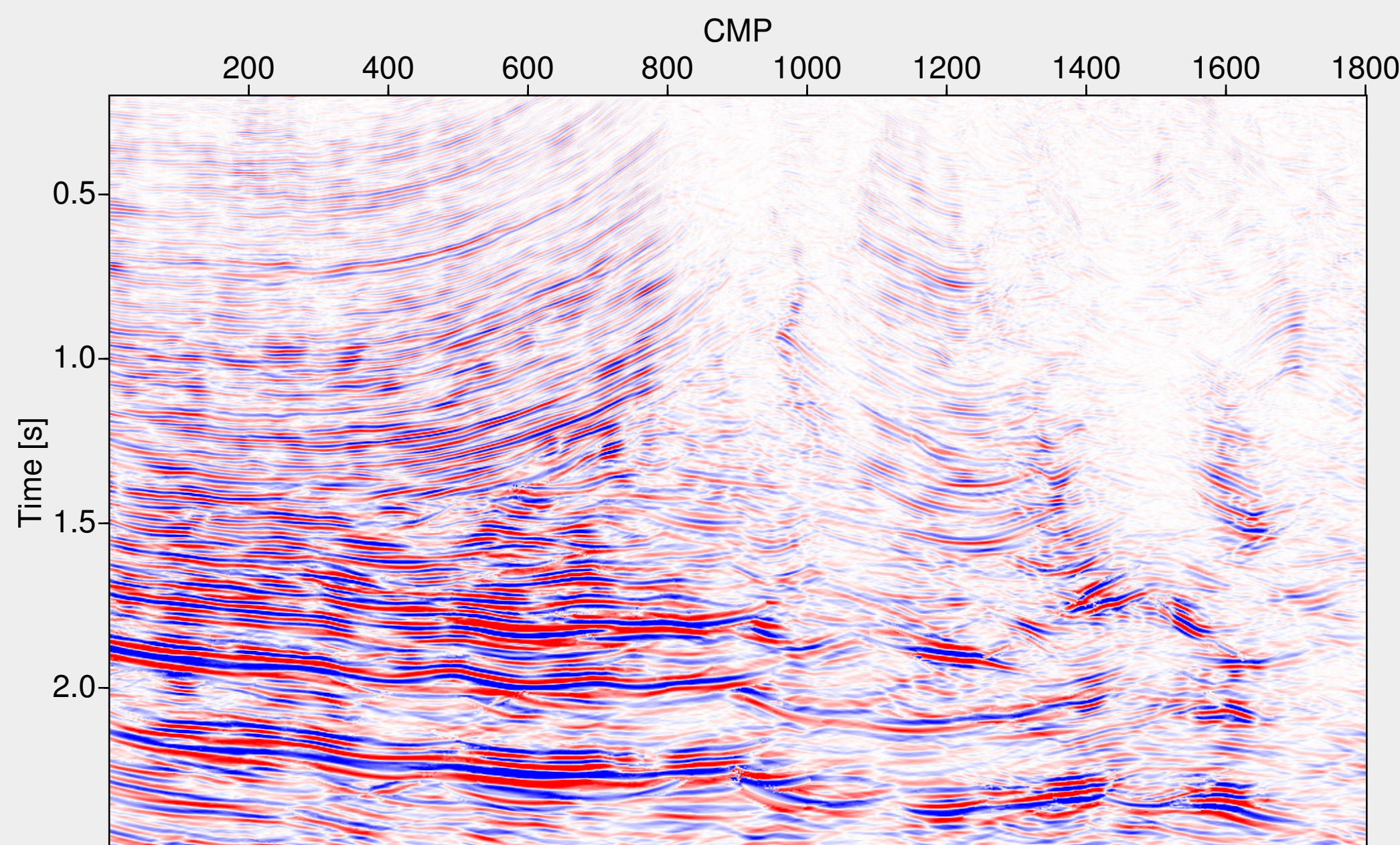


Figure 6: The result of the Kirchhoff poststack time migration with minimum aperture. The conventional aperture has been used where no stationary points have been detected.

A closer investigation of the three horizontal reflection events below 1.8 s reveals different effects in the limited-aperture migration result: on the one hand, an improved continuity of these reflection events, for instance at the reflection event between CMP nos. 200 to 400 at 2.15 s, but on the other hand unphysical fluctuations due to unreasonably strong variations of the attributes occurring around CMP no. 900 at 2.3 s. The imaging problem at this area is also complicated by conflicting dip situations which have not been considered for these data. The fluctuations occurring due to varying attributes are usually prevented by a previous event-consistent smoothing of the attributes. However, due to the poor signal-to-noise ratio and low coherence of the data set a reliable smoothing was not possible in this case.

Prestack migration results

Figure 7 shows the conventional prestack migration result after muting and stacking over all offsets, whereas in Figure 8 the corresponding result of the prestack migration with minimum aperture is depicted. As in the poststack case, the user-defined aperture was used at all locations where no stationary point was found. The differences between the two prestack results are comparable to those of the poststack results. The application of the introduced migration technique improved the computational efficiency significantly: compared to conventional migration, the reduction of the required summations led to half of the computational time in the prestack case.

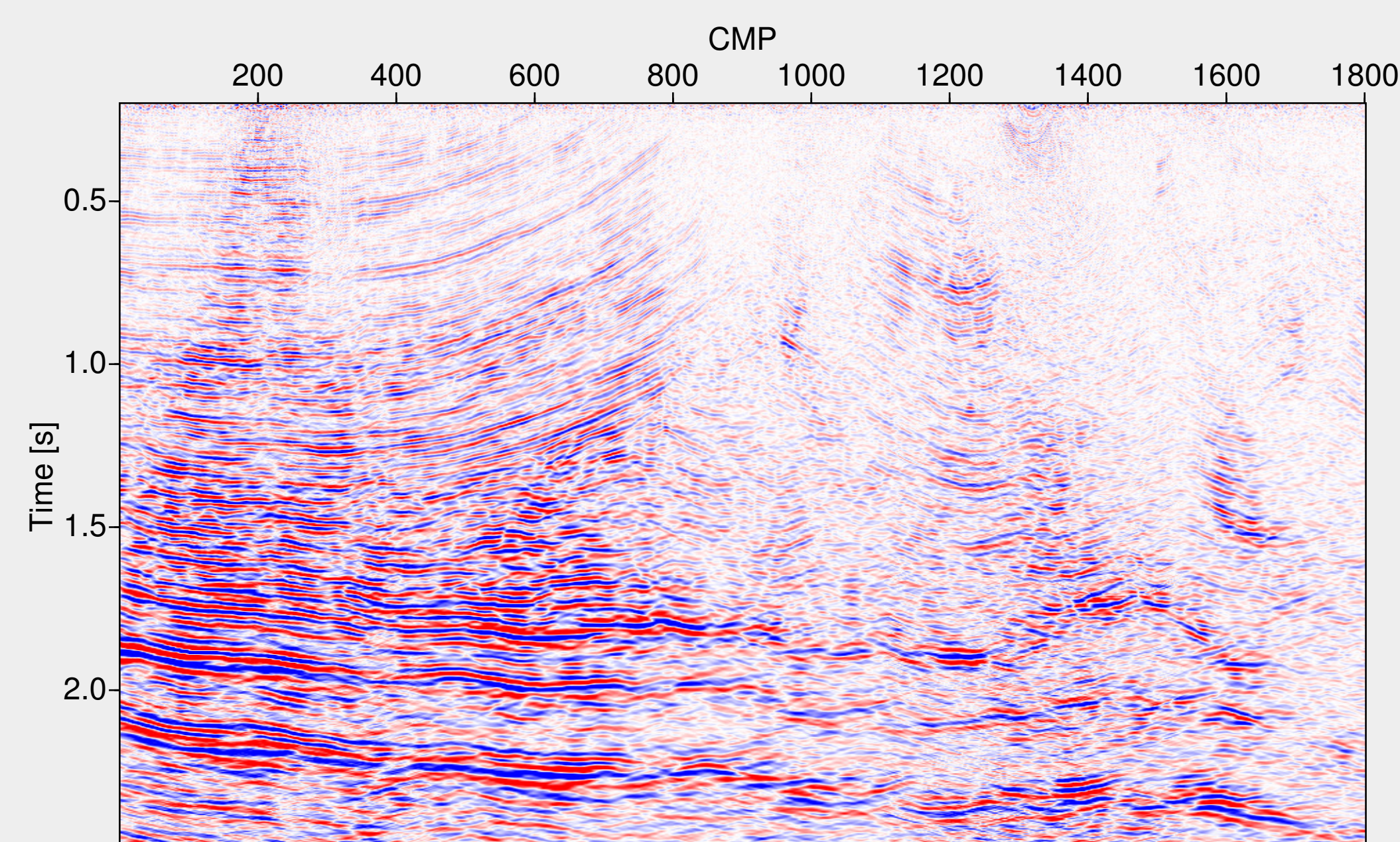


Figure 7: Result of the Kirchhoff prestack time migration with conventional user-defined aperture after stacking.

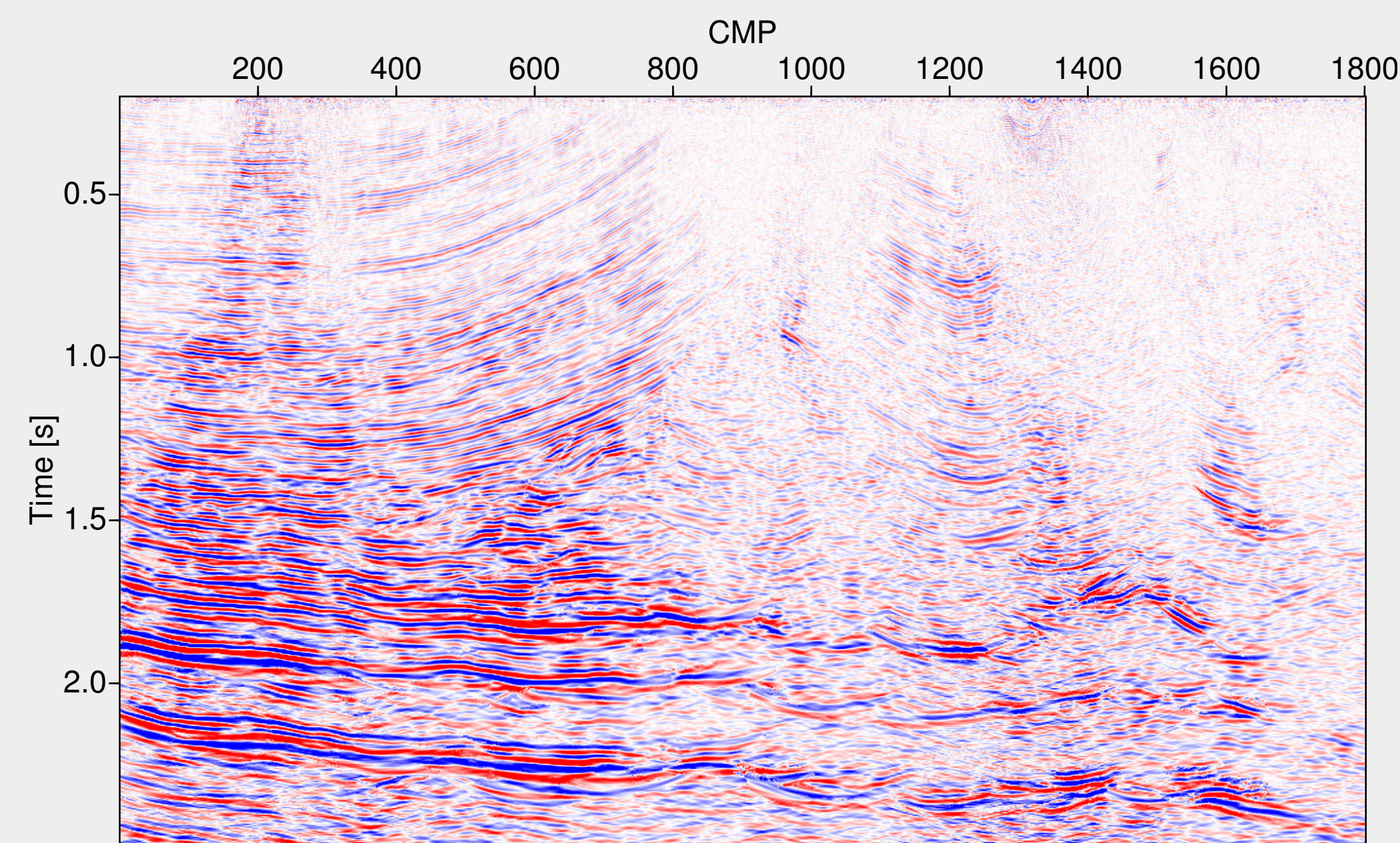


Figure 8: Result of the Kirchhoff prestack time migration with minimum aperture after stacking. The conventional aperture has been used where no stationary points have been detected.

Amplitudes versus offset

The effect on the amplitudes was analysed by extracting an AVO curves from the strong reflector in the common-image gather at CMP 560 in both, conventional and limited-aperture prestack migration results (Figure 9). A reduction of the noise-related fluctuations can be observed in the limited-aperture AVO plot as just the relevant part of the data was summed up. Hence, AVO analysis benefits from migration with limited aperture.

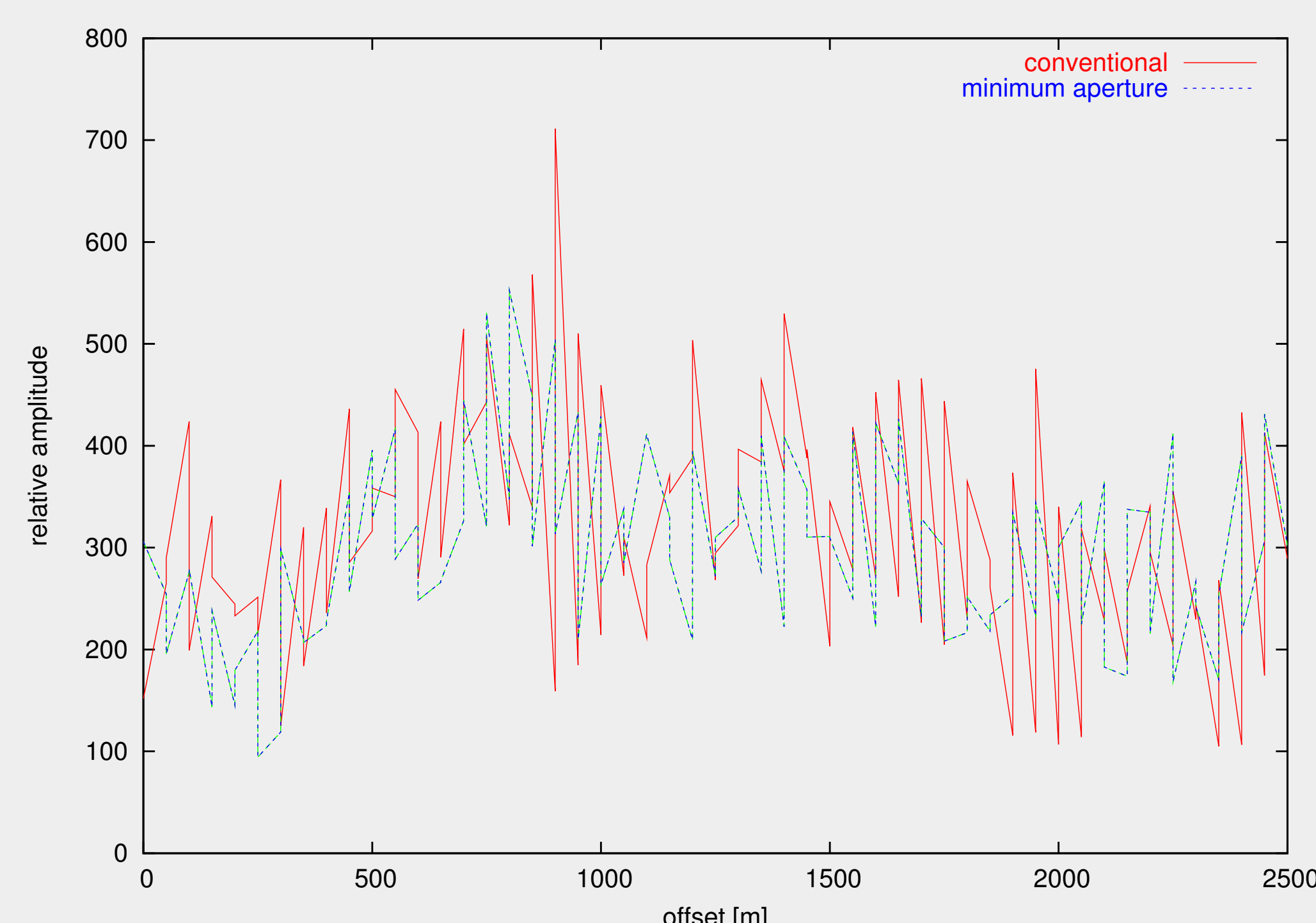


Figure 9: AVO of a strong reflector event at 1.8 s extracted in the common-image gather for CMP no. 560 after true-amplitude prestack time migration with minimum aperture (dashed line) and conventional aperture (solid line).

Transition between apertures

For data with a poor signal-to-noise ratio stationary points may not be found on every reflection event. In this case the user-defined aperture is utilised within such gaps to obtain a fully covered image. We checked whether this local jumps between minimum aperture and user-defined aperture have an impact upon the amplitudes or cause artefacts in the migration image: we enforced that the conventional aperture was used from trace number 7820 up to the last trace. The obtained migration result shows no artefacts at this artificial transition. A detail of the amplitudes extracted around trace no. 7820 is displayed in Figure 10. The local fluctuation is most likely caused by a varying noise level: an approximated spline based on these amplitude picks showed no evident variation of its character around the location. Thus, it appears that the switch between the two migration apertures does not lead to a general systematic mismatch between the respective amplitudes.

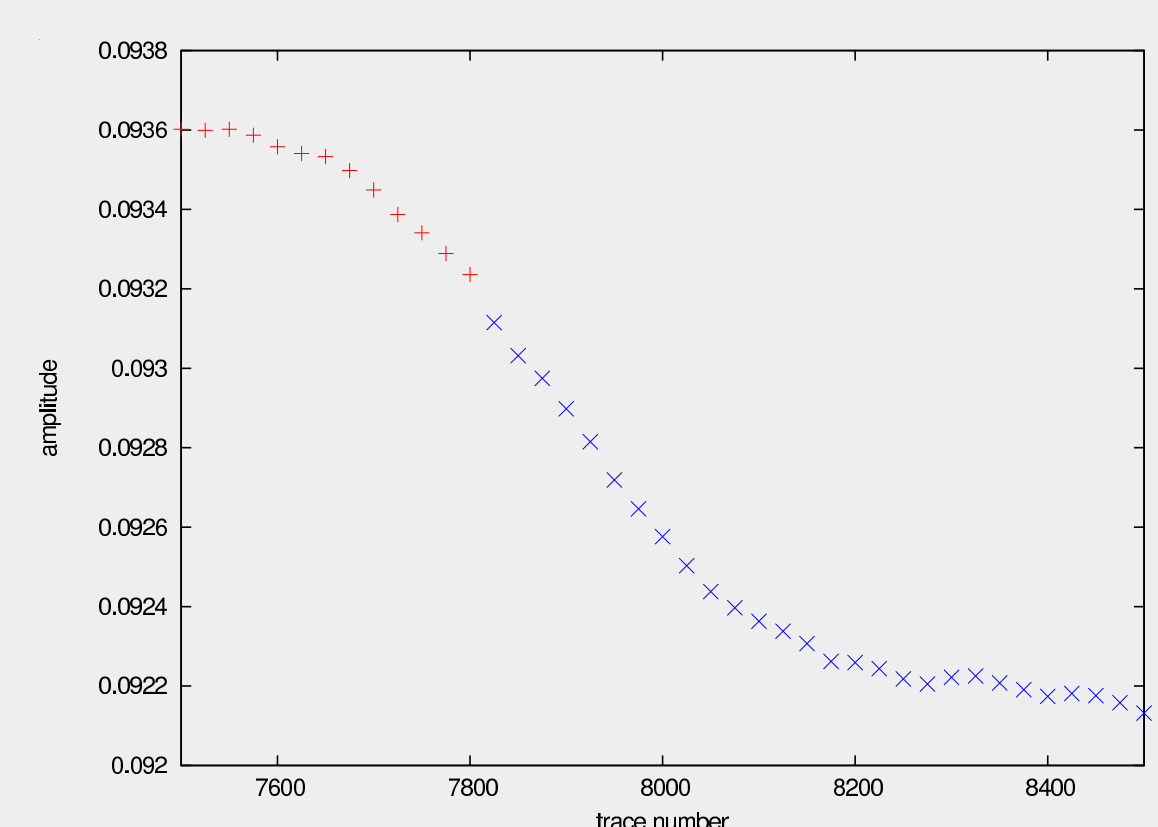


Figure 10: Amplitudes extracted around trace no. 7820 where the aperture changes from minimum aperture (red) to conventional (blue).

Conclusions

Jäger (2005) successfully applied CRS wavefield attributes for minimum-aperture Kirchhoff depth migration. Spinner and Mann (2006) demonstrated that this concept can be transferred back to the time domain. Here, not only the sensitivity to velocity model errors is reduced, but also the migration velocity model building can be performed in a highly automated and simple way. The entirely analytic migration operators and their corresponding derivatives allow an efficient implementation, especially concerning the determination of stationary points. The presented data example shows that we obtain more reliable amplitudes for AVO/AVA analyses compared to conventional approaches.

References

- Höcht, G., de Bazelaire, E., Majer, P., and Hubral, P. (1999). Seismics and optics: hyperbolae and curvatures. *J. Appl. Geoph.*, 42(3,4):261–281.
- Jäger, C. (2005). Minimum-aperture Kirchhoff migration by means of CRS attributes. In *Extended abstracts, 66th Conf. Eur. Assn. Geosci. Eng. Session F042*.
- Mann, J. (2002). *Extensions and applications of the Common-Reflection-Surface Stack method*. Logos Verlag, Berlin.
- Schleicher, J., Tygel, M., and Hubral, P. (1993). Parabolic and hyperbolic paraxial two-point traveltimes in 3D media. *Geophys. Prosp.*, 41(4):495–514.
- Spinner, M. and Mann, J. (2006). True-amplitude CRS-based Kirchhoff time migration for AVO/AVA analysis. *J. Seis. Expl.*, 15(2):133–152.

Acknowledgements

We would like to thank OMV and Gaz de France for the permission to use and publish their data. This work was supported by the sponsors of the *Wave Inversion Technology Consortium*.

Related presentations

- B044** CRS stacking: a simplified explanation, *J. Mann, J. Schleicher, and T. Hertweck*
- P058** Automatic tracking of reflection events in 3D ZO volumes using CRS attributes, *N.-A. Müller*
- H015** 2D CO CRS poststack imaging for walkaway VSP data, *M. von Steht*